A brainstem to hypothalamic arcuate nucleus GABAergic circuit drives feeding

Pablo B Martinez de Morentin*[1], J Antonio Gonzalez, Yuliia Martynova, Sergiy Sylantyev*, Lora K Heisler

The Rowett Institute, Healthy Lifecourse and Nutrition Neuroscience (HeLNN), University of Aberdeen, UK.

*Correspondence

[1]Lead contact

[1]pablo.morentin@abdn.ac.uk

s.sylantyev@abdn.ac.uk

ORCIDs:

PBM 0000-0002-0684-3215

JAG 0000-0001-7045-4831

YM 0000-0003-1927-3298

SS 0000-0002-1358-0601

LKH 0000-0002-7731-1419

Highlights

- Nucleus of the solitary tract (NTS) GABA neurons are responsive to nutritional status.
- Chemogenetic $GABA^{NTS}$ neuron activation reduces food intake and body weight.
- $GABA^{NTS}$ projections to the hypothalamic arcuate nucleus (ARC) promote satiety.
- Optogenetic $GABA^{NTS}$→ARC stimulation inhibits orexigenic AgRP/NPY neurons.

In Brief

Martinez de Morentin et al. identify GABAergic neurons in the nucleus of the solitary tract as a new player in the circuit governing feeding behavior and body weight.

Abstract

The obesity epidemic is principally driven by the consumption of more calories than the body requires. It is therefore essential that the mechanisms underpinning feeding behavior are defined. The brainstem nucleus of the solitary tract (NTS) receives direct information from the digestive system and projects to second order regions including the arcuate nucleus of the hypothalamus (ARC). Here we reveal that selective activation of NTS γ-Aminobutyric acid ($GABA^{NTS}$) neurons is sufficient to significantly control food intake and body weight. Optogenetic interrogation of $GABA^{NTS}$ circuitry identified $GABA^{NTS}$→ARC projections as appetite suppressive without creating aversion. Electrophysiological analysis revealed $GABA^{NTS}$→ARC stimulation inhibits hunger promoting agouti-related protein/neuropeptide Y (AgRP/NPY) neurons via GABA release. Adopting an intersectional genetics strategy, we clarify that the $GABA^{NTS}$→ARC circuit induces satiety. These data identify $GABA^{NTS}$ as a new modulator of feeding behavior, body weight and controller of orexigenic AgRP/NPY activity, thereby providing insight into the neural underpinnings of obesity.

Keywords

y-Aminobutyric acid, agouti-related -peptide, Neuropeptide Y, nucleus of the solitary tract, food intake.

Introduction

Obesity represents a key challenge to human health and is primarily due to the consumption of calories in excess to body's energy requirements. Eating is a complex behavior that not only depends on the basic energy demands at a cellular and organism level, but also the integration of internal and environmental cues, the reward value of food, motivation, and conditioning behavior [1,2]. The aim of the present study was to probe neurocircuitry regulating feeding and body weight with the objective of uncovering critical energy homeostasis circuitry.

One of the primary nodes for the integration of energy-related information from the periphery to the brain is the nucleus of the solitary tract (NTS) within the brainstem dorsal vagal complex (DVC) [3]. The NTS contains a heterogeneous population of energy-related sensitive cells [4–6]. Recent studies using single-nucleus RNA sequencing provide a detailed expression map of identified cellular populations involved in energy balance, and most were revealed to be glutamatergic [4,5]. For example, subpopulations of these glutamatergic cells influencing energy balance include leptin receptor (LEPR) [7], calcitonin receptor (CALCR) (Cheng, et al., 2020), glucagon-like peptide 1 receptor (GLP-1R) [9,10], preproglucagon (PPG) [11], tyrosine hydroxylase (TH) [12,13], cholecystokinin (CCK) [14] and proopiomelanocortin (POMC) [15,16]. However, very little is known about the role of NTS inhibitory GABA-releasing clusters ($GABA^{NTS}$) in energy homeostasis. One report in rats indicated a subpopulation of GLP-1R-expressing neurons releasing GABA are necessary mediators for the anorectic effects of the obesity medication liraglutide [10]. Therefore, $GABA^{NTS}$ represents and intriguing and understudied population of NTS cells and is the focus of the present study.

In the regulation of feeding behavior, one of the most widely studied projections from the NTS is to the hypothalamus [12,14,17–20]. However, whether the arcuate nucleus of the hypothalamus (ARC) receives inhibitory control from the NTS is not known. Within the ARC is a subpopulation of potent orexigenic neurons expressing both agouti-related peptide and neuropeptide Y (AgRP/NPY) [21–24]. We hypothesized that $GABA^{NTS}$ neurons significantly regulate feeding and body weight and project to and inhibit key hunger-stimulating AgRP/NPY cells.

Results

Activation of $GABA^{NTS}$ cells reduces food intake and body weight

GABA^{NTS} are expressed across the DVC and have a heterogenous neurochemical profile [4,5]. To examine whether GABA^{NTS} cells are responsive to energy status, we facilitated the visualization of GABA^{NTS} neurons by crossing *Vgat-ires-Cre* mice with *tdTomato$^{fl/fl}$* reporter mice (*Vgat^{tdTom}* **Figure 1A and 1B**). We then examined the expression levels of the neuronal activity marker c-Fos [25] in mice that were overnight fasted and in mice that were refed for 2 hours after overnight fasting (**Figure 1C**). Re-fed mice showed significantly more c-Fos in the NTS (**Figure 1D**) and specifically in GABAergic cells (**Figure 1E**) when compared to fasted mice. This suggests that GABA^{NTS} cells are responsive to positive energy status.

To determine whether GABA^{NTS} neurons have a role in the control of food intake, we used chemogenetic Designer Receptors Exclusively Activated by Designer Drugs (DREADD) to manipulate GABA^{NTS} cellular activation [26]. Specifically, AAVs expressing hM3Dq-mCherry or control mCherry were bilaterally injected into the NTS of *Vgat^{Cre}* mice (**Figure 1F**) to allow temporal activation of GABA^{NTS} neurons. Administration of designer drug clozapine-N-oxide (CNO) induced expression of c-Fos in the NTS (**Figure 1G**). Chemogenetic activation of GABA^{NTS} cells significantly reduced overall food intake during the dark cycle in mice fed ad libitum compared to saline treatment in the same mice (**Figure 1H**). Next, mice were fasted overnight to increase hunger and then treated with CNO or saline prior to the presentation of food in the light cycle. CNO significantly reduced hunger-induced refeeding as compared with saline treatment in hM3Dq-mCherry mice (**Figure 1I**).

Given that activation of GABA^{NTS} significantly reduced acute food intake, we next evaluated whether a sustained activation using daily administration of CNO (**Figure 1J**) would result in prolonged reductions in food intake and weight loss. When compared to control mCherry-expressing mice, twice-daily administration of CNO in hM3Dq-mCherry-expressing mice produced a significant reduction in daily food intake (**Figure 1K**). Similarly, treatment with CNO produced a progressive reduction in body weight in hM3Dq-mCherry-expressing mice (**Figure 1L**). Although feeding returned to normal baseline levels after 72 hours of saline administration in hM3Dq-mCherry-expressing mice, body weight remained significantly lower (**Figure 1K-L**). These results indicate that the selective activation of GABA^{NTS} neurons is sufficient to control sustained feeding behavior and body weight via reduced energy intake.

Optogenetic stimulation of GABA^{NTS} terminals inhibits AgRP/NPY^{ARC} cells

To clarify the circuitry through which $GABA^{NTS}$ neurons influence feeding and body weight, we used Channelrhodopsin 2 (ChR2)-assisted circuit mapping (CRACM) [27,28]. Specifically, we injected AAVs expressing ChR2-mCherry in the NTS of *Vgat*^{Cre} mice (**Figure 2A**) and analyzed projection patterns. $GABA^{NTS}$ cells project to hypothalamic subregions including the ARC, paraventricular nucleus (PVH) and dorsomedial nucleus (DMH) and various other extra-hypothalamic regions (**Figure S1A**). Within the ARC, we observed a dense array of projections (**Figure 2B**). This identified the ARC as a candidate second order region involved in the $GABA^{NTS}$ control of food intake and body weight.

Fasting induces activation of AgRP/NPY-expressing neurons [24] and direct AgRP/NPY neuron activation induces robust feeding [29,30]. Since GABA-releasing neurons are the main inhibitory network in the brain [31], we hypothesized that $GABA^{NTS}$ cells projecting to the ARC would target AgRP/NPY neurons to decrease food intake. To interrogate this potential $GABA^{NTS}$→$AgRP/NPY^{ARC}$ circuit, we crossed *Vgat*^{Cre} with *Npy*^{hrGFP} mice and bilaterally injected AAV-ChR2-mCherry into the NTS. We observed that a subset of NPY^{hrGFP} cell bodies were surrounded by mCherry-containing fibers (**Figure 2C**). In contrast, we didn't find terminals surrounding neurons expressing other neuropeptides involved in the regulation of food intake such as POMC neurons [32] (**Figure 2D**).

We next investigated whether this anatomical connectivity produced functional interactions between $GABA^{NTS}$ terminals and $AgRP/NPY^{ARC}$ neurons. Specifically, photostimulation of ChR2-containing axon terminals from $GABA^{NTS}$ neurons produced robust synaptic responses in 14% of AgRP/NPY cells in the ARC (**Figure 2E**). The rapid synaptic currents triggered in AgRP/NPY cells by the optical stimulation changed polarity near the equilibrium potential for chloride (**Figure 2F-G**), as expected from ionotropic GABA receptors. Light-induced currents were unexpectedly small, and their reversal potential was more positive than that expected for GABA-activated currents (about -60 mV). These effects could be explained by voltage- and space-clamp errors[33] and in turn suggest that perhaps NTS GABA terminals reach ARC NPY cells at dendrites distant from the soma. While it is not possible to directly demonstrate that this is the case, we tested whether this reasoning was justified by simulating the optogenetic activation of GABA synaptic events at distal vs proximal dendrites in a model neuron. Using a predictive neuronal model [34], we found that GABAergic post-synaptic currents become progressively smaller with their reversal potential progressively more positive, the further the GABA inputs are from the soma. (**Figure S1E-G**).

Next, we tested whether activation of GABA receptors at AgRP/NPY cells is accompanied by release of GABA from $GABA^{NTS}$ ChR2-containing terminals. We first stimulated ChR2-mCherry expressing $GABA^{NTS}$ fibers in the ARC and performed a "sniffer patch" experiment registering $GABA_AR$ single-channel openings above the NPY^{hrGFP} cells contacted by $GABA^{NTS}$ fibers (**Figure 2H**). In this experiment, the $GABA_AR$ response was isolated with a specific cocktail of antagonists (see Methods). This provides semi-quantitative monitoring of extracellular levels of GABA [35]. A burst of light directed to $GABA^{NTS}$ ChR2-containing terminals in the ARC induced single-channel openings in membrane patch in control conditions and the currents had amplitudes comparable to GABAergic inhibitory currents [35] (**Figure 2I, *top***). Application of $GABA_AR$ competitive antagonist gabazine reversibly blocked the single-channel openings (**Figure 2I, *middle and bottom*)**. The same pattern of receptor opening time was observed in all assessed patches (**Figure 2J**).

To test whether activation of $GABA^{NTS}$ terminals and increased GABA release specifically in the ARC inhibited neuronal signaling in AgRP/NPY cells, we next performed a protocol of additive subthreshold electrical stimuli. This method is designed to evoke an action potential after 5 stimuli and we coupled a 470 nm light burst to the same trigger (**Figure 2K**). We then alternated a sequence of electrical stimuli and electrical stimuli with light burst. The electrical stimulation evoked an action potential(s) (**Figure 2L, top)** and this was blocked by the light burst (**Figure 2N, bottom**) which was accompanied with single-channel openings in a sniffer patch (**Figure 2M**). These openings resembled $GABA_AR$ openings illustrated in Figure 2J. Subsequent stimulations showed a decrease in channel opening intensity, suggesting a depletion of GABA stores from the presynaptic terminal, which was eventually insufficient to prevent the action potential (**Figure S1B**). These results provide strong evidence that $GABA^{NTS}$ fibers inhibit AgRP/NPY cells due to the release of the fast neurotransmitter GABA.

$GABA^{NTS}$→ARC optogenetic stimulation reduces feeding and is not aversive

Given the dense fiber projection pattern of NTS-GABAergic cells to the ARC and that its activation induced a strong inhibition of AgRP/NPY neurons, we interrogated whether this circuit is sufficient to influence food intake. To investigate this, AAVs expressing ChR2-mCherry were infused into the NTS of $Vgat^{Cre}$ mice and an optic fiber was placed above the ARC (**Figure 3A**). Food intake was measured both without and with ARC photostimulation prior to entering the dark cycle (**Figure 3B and 3C**). Light stimulation of $GABA^{NTS}$→ARC

terminals induced a strong acute inhibition of food intake that lasted 60 min from food presentation as compared to the same mice without light stimulation (**Figure 3D and 3E**).

The DVC has been proposed to be a key region modulating food intake reductions associated with aversive states [36]. To assess whether $GABA^{NTS}$→ARC activation produces aversion or negative valence [37,38], we evaluated the existence of passive avoidance behavior using an adapted real-time place preference (RTPP) task [14,39,40]. Specifically, in a two-sided open arena, light stimulus was coupled to one of the sides (**Figure 3F**). $GABA^{NTS}$→ARC stimulation or lack of stimulation did not produce a place preference (**Figure 3G**) and mice travelled a similar distance in both sides of the arena (**Figure 3H**). These findings indicate that $GABA^{NTS}$→ARC stimulation does not produce negative valence or aversion.

In addition to influencing homeostatic feeding, modulation of AgRP/NPY cells has also been reported to elicit anxiety-like behaviors influencing exploration and foraging which impacts food consumption [41–43]. To test whether the activation of the $GABA^{NTS}$→ARC circuit produced anxiety-related behavior, mice were assessed in an open-field arena (OFA) and an elevated zero-maze task (EZM) (**Figure S2A and S2D**). $GABA^{NTS}$→ARC stimulation did not alter the time mice spent in the center of the OFA (**Figure S2B**). Likewise, mice displayed similar ambulatory patterns and travelled comparable distance during the OFA test with and without $GABA^{NTS}$→ARC stimulation (**Figure S2C**). Consistent with the OFA data, $GABA^{NTS}$→ARC stimulation did not alter either the time (**Figure S2E**) or distance travelled in the exposed zones of the EZM (**Figure S2F**). These results provide evidence that stimulation of the $GABA^{NTS}$→ARC circuit impacts feeding without altering other behavioral states such as anxiety-like behavior.

We postulated that since our model involved fast neurotransmission rather than long term release of neuropeptides, the reduction in food intake that we observed could begin by reducing the interaction with the nutritional cue at first instance. To investigate this, we designed a task where mice would first be allowed to explore an empty arena and then three items would be presented at the same time, an inedible object, a novel palatable food item and a known nutritional food item (**Figure 3I**). The number of interactions with each item was measured with and without $GABA^{NTS}$→ARC stimulation. $GABA^{NTS}$→ARC stimulation did not induce changes in the interaction with the novel object (**Figure 3J**), further suggesting that $GABA^{NTS}$→ARC does not induce anxiety-like behavior. The number of interactions with the novel palatable food item was increased under both non-stimulation and stimulation trials

(**Figure S2F and S2G**). However, we found that under optical stimulation mice had less interactions with the known nutritional item (**Figure 3J and S2G**), suggesting that $GABA^{NTS}$→ARC activation reduces hunger. Taken together, these findings indicate that $GABA^{NTS}$→ARC stimulation decreases feeding and hunger without inducing aversion or anxiety.

$GABA^{NTS}$→ARC neuron activation promotes satiety

We next used a two-virus intersectional approach [44,45] to provide a more detailed characterization of $GABA^{NTS}$→ARC activation in energy homeostasis. *$Vgat^{Cre}$* mice were bilaterally injected with AAVs expressing Flipase recombinase (FlpO) (AAV-DIO-FlpO) under the control of Cre into the NTS of *$Vgat^{Cre}$* mice, allowing us to express a second recombinase only in $GABA^{NTS}$ cells. After surgery recovery, a retrograde AAV encoding for a FlpO dependent hM3Dq-mCherry (rgAAV-fDIO-hM3Dq-mCherry) was bilaterally injected into the ARC to retrogradely deliver hM3Dq in a FlpO-dependent manner to $GABA^{NTS}$ cells. Therefore, hM3Dq was expressed only in $GABA^{NTS}$ cells projecting to the ARC in *$Vgat^{Cre}$* mice (**Figure 4A**).

Corroborating the optogenetic data presented above, the selective chemogenetic stimulation of the $GABA^{NTS}$→ARC circuit significantly reduced acute food intake (**Figure 4B** and **4C**) in ad libitum fed mice. $GABA^{NTS}$→ARC circuit activation did not alter overall locomotor activity (**Figure 4D** and **4E**), respiratory quotient (**Figure 4F** and **4G**) or heat production (**Figure 4H** and **4I**). $GABA^{NTS}$→ARC neuron activation also reduced food intake in refed mice after overnight fasting (**Figure 4J**). Fasting is associated with a rise in systemic levels of ghrelin [46] which acts as a pre-prandial effector stimulating AgRP/NPY neurons to initiate a feeding response [47,48]. To examine whether $GABA^{NTS}$→ARC neuron activation is sufficient to dampen a hunger cue, $GABA^{NTS}$:hM3Dq-expressing mice were pre-treated with CNO prior to ghrelin. Activation of the $GABA^{NTS}$→ARC neurons with CNO prevented the feeding induced by an orexigenic dose of ghrelin (**Figure 4L and 4M)**. We next performed an analysis of the microstructure of the feeding event during the anorectic episode produced by CNO [49–51]. $GABA^{NTS}$→ARC neuron activation reduced meal size (**Figure 4N**) and significantly reduced the number of meal events in the earliest interval compared to saline treatment (**Figure 4O** and **4P**). Taken together, these findings indicate that $GABA^{NTS}$→ARC neuron activation is

sufficient to blunt fasting and ghrelin-induced hunger and significantly reduces food intake by promoting satiety.

Discussion

Here we aimed to define critical new brain circuits modulating appetite and body weight. We focused on the NTS because it is a brain region positioned to receive and integrate energy-related information from the periphery and relay it within the CNS to promote energy homeostasis. However, the NTS is neurochemically heterogeneous and key neurons within it performing this function have not been fully defined. Using multi-methodological approach, here we identify $GABA^{NTS}$ neurons as sufficient to control feeding behavior and body weight in mice.

Recent efforts to decode the function of specific chemically defined neurons within the NTS have revealed that distinct subpopulations of glutamatergic cells play a role in energy homeostasis[5]. However, NTS inhibitory GABA-releasing neurons have not been studied in detail and this is necessary to clarify the role of both excitatory and inhibitory NTS signals in the regulation of energy balance [52]. Here we provide a detailed characterization of the effect of $GABA^{NTS}$ in the regulation of energy homeostasis and body weight. A recent report provided evidence that obesity medication liraglutide engages $GABA^{NTS}$ neurons to reduce food intake, providing a rationale that activating $GABA^{NTS}$ cells may have translational relevance for the treatment of human obesity [10].

The NTS is involved in satiety and satiation, and refeeding induces a strong neuronal activation in this region [14,53]. We discovered that refeeding significantly activates a subset of $GABA^{NTS}$ cells. Further, we found that activation of $GABA^{NTS}$ neurons with chemogenetics controlled daily food intake and body weight. How the NTS coordinates and transmits satiety and satiation to the brain is not fully understood. Our data illustrates that $GABA^{NTS}$ neurons project widely within the brain, with particularly dense innervation of the hypothalamus. Several studies indicate that there is a coordination between the NTS and the hypothalamus to orchestrate the meal event [12,18–20,54]. However, whether the ARC receives inhibitory control from the NTS is not known and was examined here.

Given that GABA is an inhibitory neurotransmitter, we hypothesized that $GABA^{NTS}$ neurons inhibit appetite stimulating neurons. We focused on $AgRP/NPY^{ARC}$ neurons because of the

dense $GABA^{NTS}$ innervation of the ARC and the potent orexigenic properties of AgRP/NPY [30,55,56]. We demonstrated that $GABA^{NTS}$ terminals in the ARC release GABA and that this is synchronized with suppression of the action potential propagation postsynaptic $AgRP/NPY^{ARC}$ cells. The timescale of $GABA_AR$ openings after optical stimulation in a membrane patch placed over the $GABA^{NTS}$ terminal suggests the release of GABA via $GABA_ARs$. The number of AgRP/NPY neurons responding is in line with the 20% ARC responders to NTS innervation published previously [12]. However, despite the relatively small number of $AgRP/NPY^{ARC}$ neurons inhibited by $GABA^{NTS}$ terminals, it was sufficient to significantly reduce feeding in freely behaving mice. AgRP/NPY cells are poised to orchestrate the integration of homeostatic, reward and sensory cues as well as learning and conditioned behaviors [30,42,55,57–64]. A detailed analysis of feeding behavior revealed that activation of the $GABA^{NTS}$→ARC pathway specifically reduces hunger and promotes satiety and does not induce negative valence, aversion or anxiety.

Obesity is an international health concern that is primarily the consequence of over-eating. Defining the mechanisms governing hunger and food intake is therefore of paramount importance. Here we identify a new player that potentially controls appetite and body weight, $GABA^{NTS}$. Specifically, we show that NTS GABA-releasing neurons are active during satiety and reduce food intake and body weight without causing aversion or anxiety. We demonstrate that $GABA^{NTS}$ cells directly activate $GABA_ARs$ on the surface of AgRP/NPY cells which inhibits neuron activity. These studies reveal for the first time the effect of $GABA^{NTS}$ neurons on feeding and body weight and identify a fast inhibitory circuit between the NTS and the ARC in the control of food intake. These results thereby provide significant insight into the brain circuits governing appetite and body weight, findings of relevance to the global obesity crisis.

Methods

Animals

Vgat-ires-Cre [65] (Slc32a1tm2(cre)Lowl; #016962), *NPY-hrGFP* [66] (B6.FVB-Tg(Npy-hrGFP)1Lowl/J; #006417) and *Rosa26tdTomato-LoxP* [67] (B6.Cg-Gt(ROSA)26Sortm9(CAG-tdTomato)Hze/J, #007909) mice were obtained from The Jackson Laboratory (Bar Harbor, USA) and bred in a C57Bl/6J background. Mice were fed with standard laboratory chow (Standard CRM (P) 801722, Special diets, UK) and provided with water ad libitum, unless otherwise stated. Mice were kept in a 12-hours light:dark cycle (7am-7pm) in environmental controlled conditions (20-22°C and 40-60% RH). All experimental procedures were performed in accordance with the UK Animal (Scientific Procedures) Act 1986.

Viral vectors

Cre-dependent viral vectors were purchased from Addgene, AAV8-hSyn-DIO-hM3D(Gq)-mCherry ($1.83x10^{12}$ gc/ml) was a gift from Bryan Roth (Addgene plasmid # 44361) [30], AAVrg-hSyn-fDIO-hM3D(Gq)-mCherry-WPREpA ($1.8x10^{12}$ gc/ml) was a gift from Ulrik Gether (Addgene plasmid # 154868); AAV8-hSyn-DIO-mCherry ($3.6x10^{12}$ gc/ml) was a gift from Bryan Roth (Addgene plasmid # 50459); AAV8-pEF1a-DIO-FLPo-WPRE-hGHpA ($2x10^{12}$ gc/ml) was a gift from Li Zhang (Addgene plasmid # 87306) [68]. AAV2-EF1a-DIO-ChR2(E123T/T159C)-mCherry ($7.3x10^{12}$ vp/ml) was a gift from Karl Deisseroth and were obtained from University of North Carolina Vector Core (Chapel Hil, NC, USA). All viral particles were delivered into nuclei-specific regions through stereotaxic injections.

Stereotaxic surgeries

For viral delivering in the NTS, stereotaxic surgery was adapted from previous studies [14]. Briefly, 12-20 weeks old mice were anaesthetized with isoflurane, back region of the neck shaved and placed in a stereotaxic instrument (David Kopf instruments, CA, USA) with a face mask (World Precision Instruments, FL, USA). Head was inclined ~70 degrees forward and a longitudinal incision was made in the skin at the level of the C1; neck muscles were retracted to expose the atlanto-occipital membrane. This was carefully dissected allowing access to the dorsal brainstem and visualization of the obex. Using a pulled glass capillary

(40μ tip diameter) (G1, Narishige, UK) and a pneumatic microinjector (IM-11-2, Narishige, UK) 200-300 nl of viral preparation was bilaterally injected into the NTS (obex: AP:0.25 mm AP, L:± 0.25 mm and DV:-0.25mm) at a flow of 50nl/min. Capillary was left in the injection place for 5 min to allow diffusion and it was removed slowly to avoid dispersion to neighbor brainstem regions. Viral delivery into the ARC was performed as previously described [69] at coordinates bregma: AP:1.58 mm AP, L:±0.2mm and DV:5.90 mm. For optical fiber cannula placement, mice were allowed 4 weeks recovery form the NTS surgery and a 200 μm core diameter, 0.39NA (CFMLC, Thorlabs, UK) optical fiber implants were placed in the third ventricle above the ARC. Mice were allowed 3 weeks before any study to allow surgery recovery and maximal viral expression. Post hoc analysis of injection site, viral expression and canula placement were used as exclusion criteria for data analysis.

Photostimulation protocol

Optical fiber implants were attached to optogenetics patch cables (M83L1, Thorlabs, UK) connected to a rotary joint (Doric lenses) coupled to a 473-nm laser (Laserglow, Toronto, Canada) controlled via TTL-USB interface with Arduino board. For feeding experiments, the stimulation protocol was 1 s followed by 4 s break with 10ms light pulses with a frequency of 30Hz. For behavioral experiments, the stimulation protocol was 1 s followed by 0.5 s break with 10ms light pulses with a frequency of 30Hz. We used 15mW of laser power to achieve an irradiance of 5-10mW/mm^2 (PM100D, Thorlabs) on the target area following https://web.stanford.edu/group/dlab/cgi-bin/graph/chart.php, above ChR2 threshold activation [70].

Food intake and body weight studies

For food intake, body weight and metabolic parameters measurements, mice were single housed and habituated in indirect calorimetry system cages for one week (Phenomaster, TSE Systems, Germany). For acute ad libitum studies, access to food was removed in fed mice 2h before entering the dark cycle and CNO 1 mg/kg was i.p. administered 30 min before the dark cycle onset when food was provided. For re-feeding studies, 12 hours dark cycle-food deprived mice were i.p. injected with CNO at the beginning of the light cycle and 30 min after

food was provided. For subchronic studies, mice were i.p. injected twice a day (am and pm) for 5 days with CNO following 5 days with saline.

Behavioral tests

For valence studies, mice were assessed in an adapted real-time place preference task consisting in an open field arena with two connected identical chambers (30x25cm) [14,39,40], one of them paired with optogenetic stimulation where mice were allowed free movement for 20 min. For anxiety tests, mice were placed in an open arena (50x50cm) with virtual delimited central and peripheral regions and allowed free movement for 10 minutes with and without stimulation in different days. For anxiety and fear assessment, mice were placed in an elevated zero maze (diameter 50cm, elevation 70 cm) with 2 hidden and 2 exposed zones and allowed free movement between zones for 10 min. Tests were performed for each animal with and without stimulation in different days. Time and locomotor parameters for each task and zone were recorded using Any-Maze software (Stoelting, IL, USA).

Immunohistochemistry and imaging

All mice were injected with a terminal dose of anesthesia and transcardially perfused with phosphate-buffered saline (PBS) followed by 10% neutral buffered formalin. Brains were dissected, post-fixed 12 hours in formalin at 4°C, cryoprotected 48 hours with 30% sucrose 4°C and coronally sectioned in 5 series at 25 µm using a freezing microtome (8000, Bright Instruments, UK). Sections were kept in protective anti-freeze solution at 4°C until they were processed for immunohistochemistry as previously described [71]. Briefly, NTS sections were washed with PBS-0.2% Tween20 30 min and then PBS (3x10 min), blocked with 1%BSA/5%DS/0.25%Triton X-100 1 hour at room temperature and incubated with primary antibody in blocking solution with anti-c-Fos (1:2500, 2250, CST, USA), anti- c-Fos (for chromogenic) (1:5000, ABE457,Merck, UK), anti-mCherry (1:2000, AB0040-200, Scigen, PT), anti-RFP (1:1000, 600-401-379, Rockland Immunochemicals, USA), anti-POMC (1:3000, H-029-30, Phoenix Pharmaceuticals, USA), anti-hrGFP (1:2000, 240141, Agilent, USA), anti-TH (1:2000, MAB318, Merck, Germany) 16 hours at room temperature. The next day, sections were washed with PBS-Tween and PBS and incubated 1 hour with appropriate secondary antibodies in blocking solution (1:500, AlexaFluor594, AlexaFluor488, Invitrogen,

UK) at room temperature. For c-Fos expression quantification in fast vs refed study, chromogenic staining with DAB reagent was performed as previously described [14].

Images were acquired using Axioskope2 microscope and Axiovision software (Zeiss, Germany). All images were converted to 8-bit, recolored and cells counted using ImageJ (Fiji).

Electrophysiology

CRACM study

CRACM experiments were performed as previously described [28]. Six (3 male and 3 female) *Vgat*^{Cre}:*Npy*^{hrGFP} mice bilaterally injected AAV-ChR2-mCherry into the NTS, aged between 5 and 7 months at the time of the electrophysiology experiments, were used. Expression of mCherry-ChR2 was targeted to NTSGABA cells by stereotaxic injection of AAV as above. Coronal brain sections 180-µm thick were prepared from these mice at least 8 days after virus injections and were placed in a bath solution consisting of (in mM) 125 NaCl, 2.5 KCl, 1.2 NaH_2PO_4, 21 $NaHCO_3$, 1 glucose, 2 $MgCl_2$, 2 $CaCl_2$. GFP-expressing cells in the ARC were identified using an upright microscope (Scientifica S-Scope-II) equipped with the appropriate fluorescence filters. Whole-cell recordings from these cells were obtained with glass pipettes (World Precision Instruments 1B150F-4) filled with a solution containing (in mM) 120 K-gluconate, 10 HEPES, 10 KCl, 1 EGTA, 2 MgCl2, 4K2ATP, and 1 Na2ATP, tip resistance 3-7 MOhm. Data was acquired using Axon Instruments hardware (MultiClamp 700B, Digidata 1550). To test for GABA inputs to AgRP/NPY^{ARC} cells, the membrane potential in these cells was clamped at increasing levels of voltage (from -100 to -10 mV in 10-mV increments), while ChR2-expressing terminals were stimulated by a single light pulse (CoolLED pE-4000) to induce post-synaptic currents. Liquid junction potential, estimated to be 10 mV, was subtracted from the measurements. Chloride equilibrium potential was calculated to be -60.3 mV.

Sniffer-patch recordings

Transverse hypothalamic slices from *Vgat*^{Cre}:*Npy*^{hrGFP} mice bilaterally injected AAV-DIO-ChR2-mCherry were cut at 200-250 using a Leica VT1200S vibratome. Slices were incubated

for one hour in a solution containing (in mM): 124 NaCl, 3 KCl, 1 $CaCl_2$, 3 $MgCl_2$, 26 $NaHCO_3$, 1.25 NaH_2PO_4, 10 D-glucose, and bubbled with 95/5% O_2/CO_2, pH 7.4. After incubation, slices were transferred to a recording chamber continuously superfused with an external solution. The external solution composition differed from incubation solution in containing 2 mM $CaCl_2$ and 2 mM $MgCl_2$.

In all experiments the intracellular pipette solution for voltage-clamp recordings contained (mM): 117.5 Cs-gluconate, 17.5 CsCl, 10 KOH-HEPES, 10 BAPTA, 8 NaCl, 5 QX-314, 2 Mg-ATP, 0.3 GTP; for current-clamp recordings: 126 K-gluconate, 4 NaCl, 5 HEPES, 15 glucose, 1 $MgSO_4 \cdot 7H_2O$, 2 BAPTA, 3 Mg-ATP (pH 7.2, 295-310 mOsm in both cases); pipette resistance was 7-9 MOhm; recordings were performed at 33-35ºC using Multiclamp-700B amplifier with -60 or -70 mV holding current (for voltage-clamp recordings); signals were pre-filtered and digitized at 10 kHz. In experiments where transmembrane currents were recorded in outside-out patches only (sniffer-patch recordings), the $GABA_A$ receptors response was isolated with a ligands cocktail containing 50 μM APV, 20 μM NBQX, 50 nM CGP-55845, 200 μM S-MCPG, 10 μM MDL-72222, and 1 μM strychnine.

Statistics and data analysis

Statistical analyses were performed using GraphPad Prism 9 software and are described in the figure legend where 2-tail paired and unpaired Student t-test were used when comparing 2 groups and RM/two-way ANOVA test with Bonferroni post-hoc correction when comparing 4 groups. No statistical method was used to predefine sample size, randomization and blinding was performed for histological quantifications. Statistical significance was accepted when the p-value was lower than 0.05. Raw data was stored in Excel and figures assembled with CorelVector and Affinity Designer software.

Author Contributions

The project was conceived by PBM and LKH. PBM designed and performed experiments and analyzed data with assistance from YM; SS and AG designed and performed

electrophysiological recordings. The manuscript was drafted by PBM with input from all other authors.

Acknowledgements

We gratefully acknowledge Dr F. Naneix for advice on optogenetics and editorial advice, and staff within the University of Aberdeen Medical Research Facility and the Microscopy Facility for their technical assistance. This work was supported by the ERC (MSCA-IF-NeuroEE-660219) to PBM, Wellcome Trust Institutional Strategic Support Fund (204815/Z/16/Z) to PBM and LKH, and the Biotechnology and Biological Sciences Research Council (BB/V010557/1) to JAG and (BB/V016849/1) to LKH and SS.

Conflict of interest

The authors declare no competing financial interests.

Figures

Figure 1

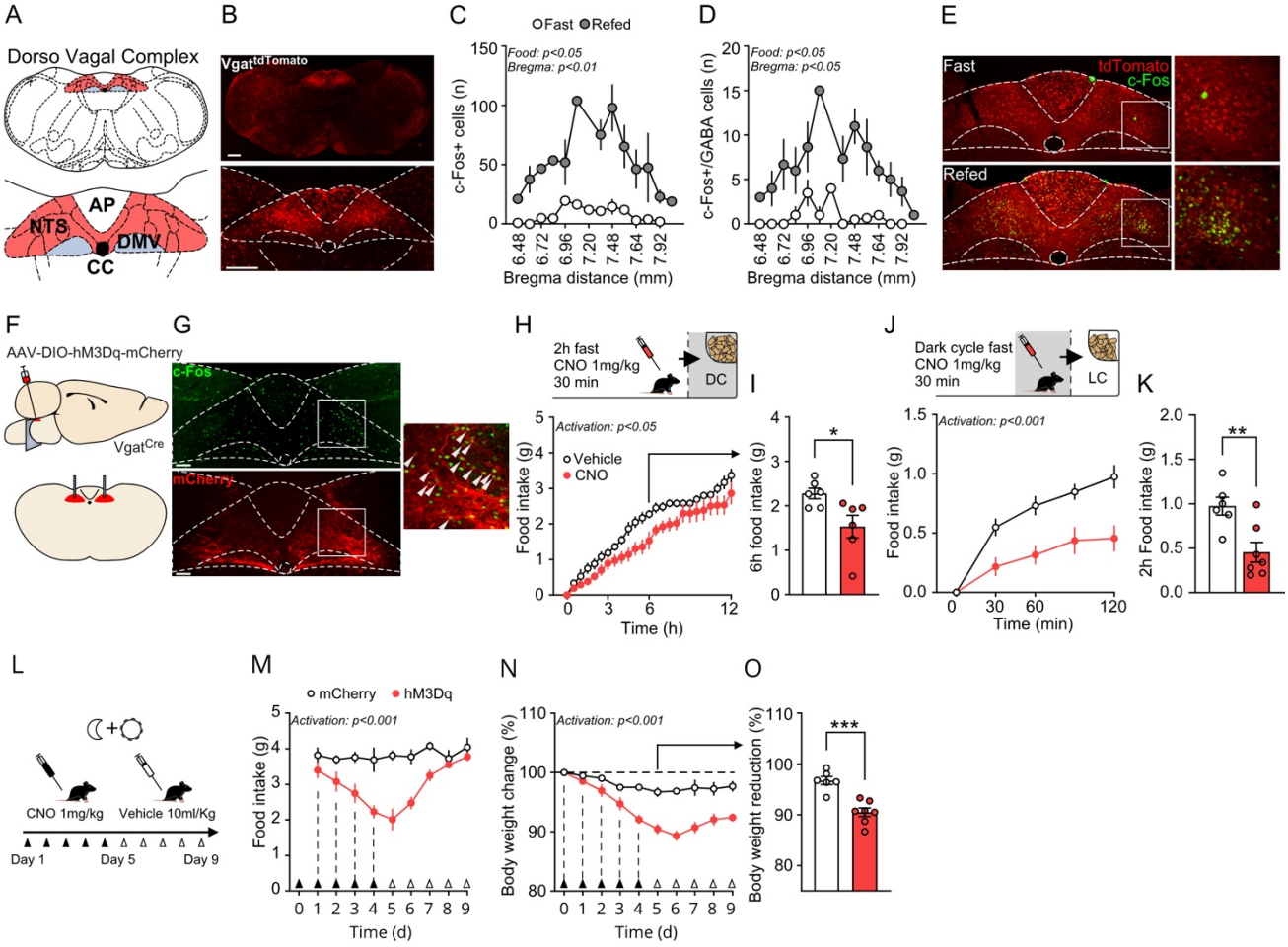

Figure 2

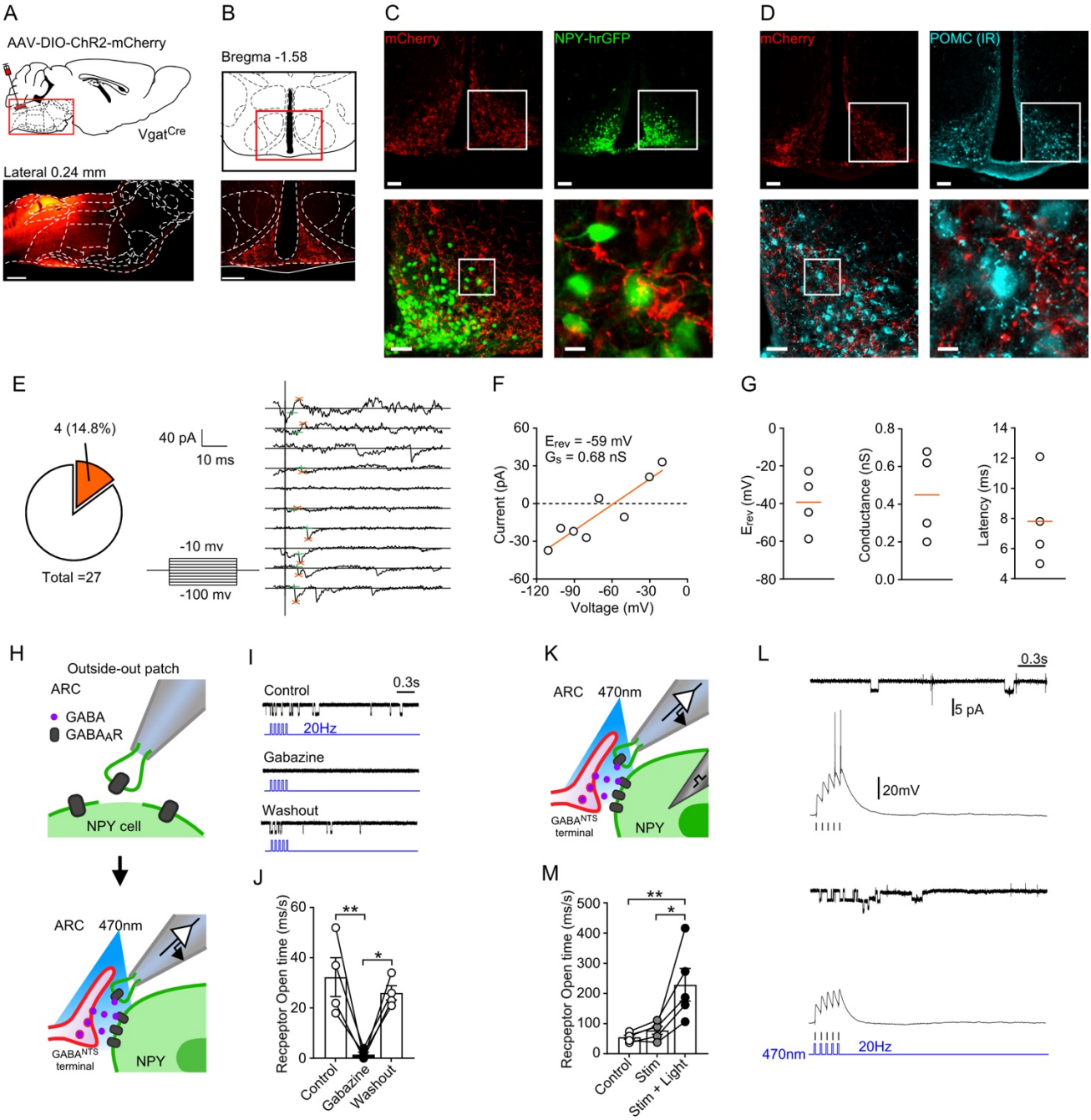
A
AAV-DIO-ChR2-mCherry
VgatCre
Lateral 0.24 mm
B
Bregma -1.58
C
mCherry
NPY-hrGFP
D
mCherry
POMC (IR)
E
4 (14.8%)
Total =27
40 pA
10 ms
-10 mv
-100 mv
F
Erev = -59 mV
Gs = 0.68 nS
Current (pA)
Voltage (mV)
G
Erev (mV)
Conductance (nS)
Latency (ms)
H
Outside-out patch
ARC
GABA
GABAAR
NPY cell
ARC 470nm
GABANTS terminal
NPY
I
Control
0.3s
20Hz
Gabazine
Washout
J
Recpeptor Open time (ms/s)
Control
Gabazine
Washout
K
ARC 470nm
GABANTS terminal
NPY
L
0.3s
5 pA
20mV
470nm
20Hz
M
Recpeptor Open time (ms/s)
Control
Stim
Stim + Light

Figure 3

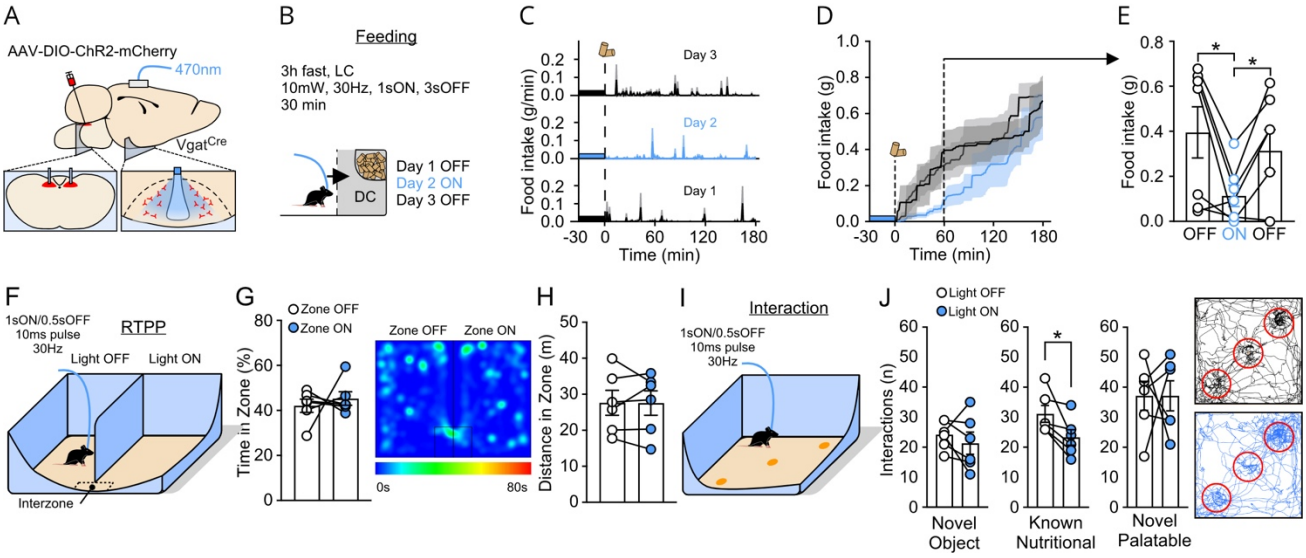
A
AAV-DIO-ChR2-mCherry
470nm
VgatCre
B
Feeding
3h fast, LC
10mW, 30Hz, 1sON, 3sOFF
30 min
DC
Day 1 OFF
Day 2 ON
Day 3 OFF
C
Food intake (g/min)
Day 3
Day 2
Day 1
Time (min)
D
Food intake (g)
Time (min)
E
Food intake (g)
OFF ON OFF
F
1sON/0.5sOFF
10ms pulse
30Hz
RTPP
Light OFF
Light ON
Interzone
G
Zone OFF
Zone ON
Time in Zone (%)
0s
80s
H
Distance in Zone (m)
I
Interaction
1sON/0.5sOFF
10ms pulse
30Hz
J
Light OFF
Light ON
Interactions (n)
Novel Object
Known Nutritional
Novel Palatable

Figure 4

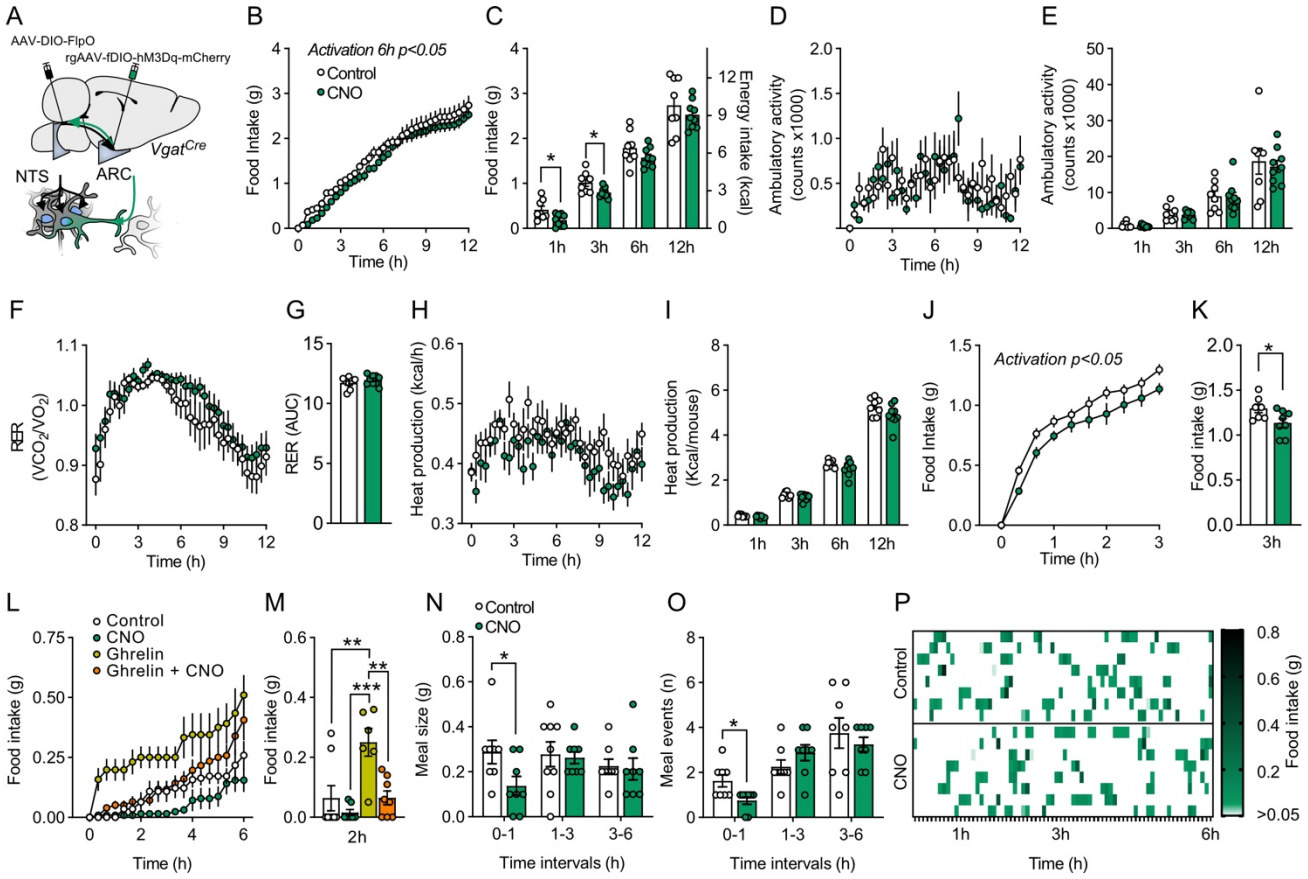
A
AAV-DIO-FlpO
rgAAV-fDIO-hM3Dq-mCherry
VgatCre
NTS
ARC
B
Activation 6h p<0.05
Control
CNO
Food Intake (g)
Time (h)
C
Food intake (g)
Energy intake (kcal)
1h
3h
6h
12h
D
Ambulatory activity (counts x1000)
Time (h)
E
Ambulatory activity (counts x1000)
F
RER (VCO2/VO2)
Time (h)
G
RER (AUC)
H
Heat production (kcal/h)
Time (h)
I
Heat production (Kcal/mouse)
J
Activation p<0.05
Food Intake (g)
Time (h)
K
Food intake (g)
3h
L
Control
CNO
Ghrelin
Ghrelin + CNO
Food intake (g)
Time (h)
M
Food intake (g)
2h
N
Control
CNO
Meal size (g)
0-1
1-3
3-6
Time intervals (h)
O
Meal events (n)
Time intervals (h)
P
Control
CNO
Food intake (g)
>0.05
1h
3h
6h
Time (h)

Supplementary Figure 1

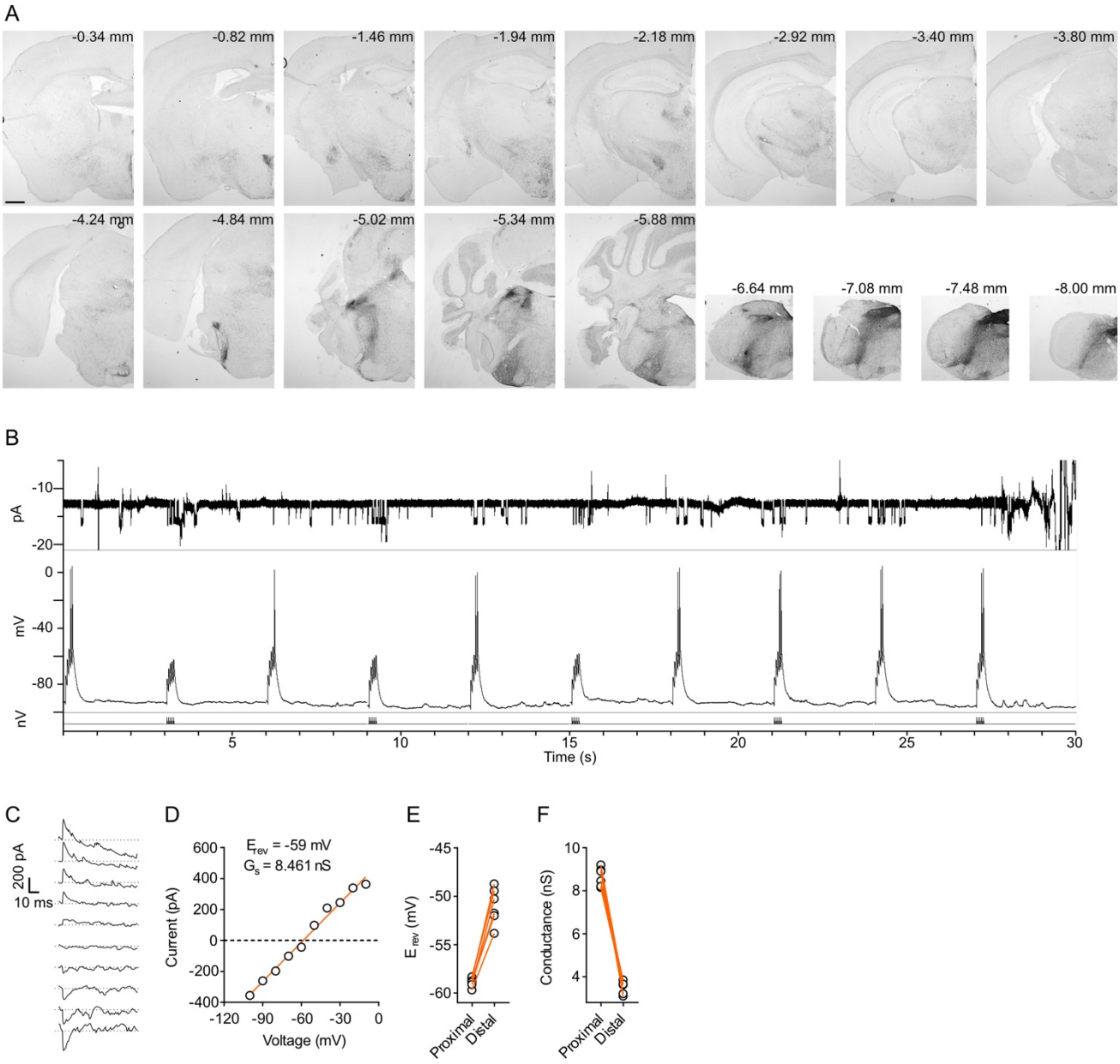

Supplementary Figure 2

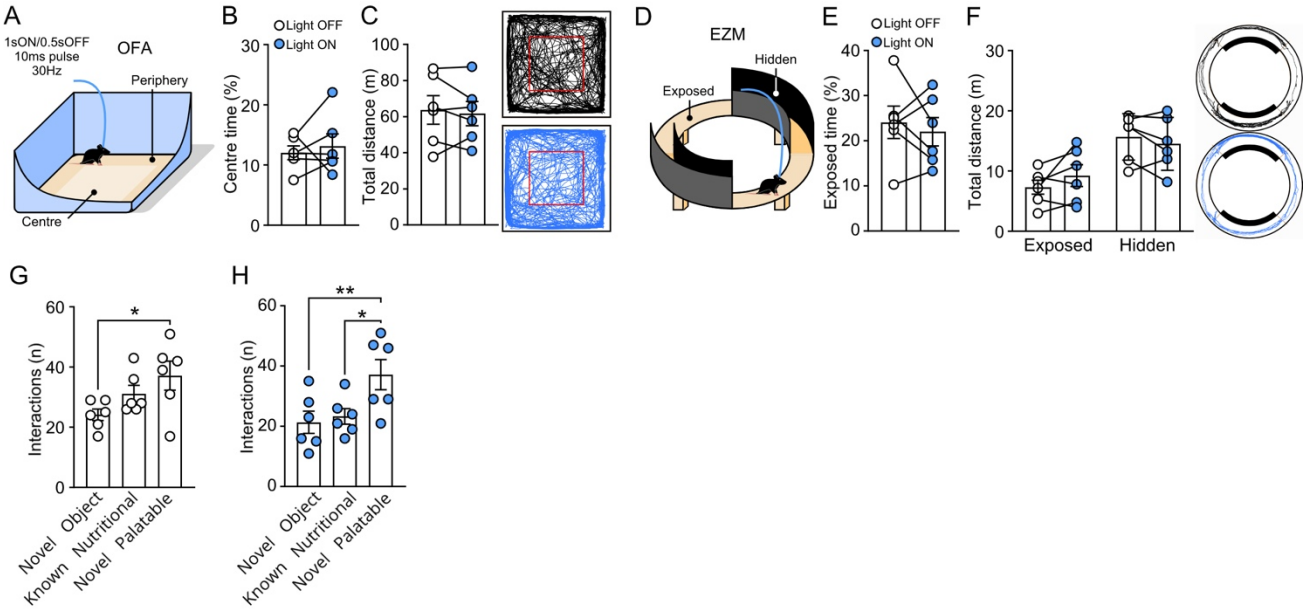

Figures Legends

Figure 1. GABA^{NTS} activation reduces food intake and body weight. (A) Schematic of the DVC (top) with zoom-in diagram showing AP, NTS and DMC (bottom). (B) Representative photomicrograph of GABAergic cell distribution in the medial brainstem (top) and in the DVC (bottom) using *Vgat^{tdTom}* mice. (C) Quantification of total NTS c-Fos-expressing cells following 16h fasting and fasting+2h refeeding (n=3, Bregma level: two-way ANOVA $F_{(13,34)}$=3.16; p=0.004; Nutritional state: two-way ANOVA $F_{(1,4)}$=18.61; P=0.012). (D) Quantification GABAergic cells expressing c-Fos following 16h fasting and fasting+2h refeeding (n=3, Bregma level: two-way ANOVA $F_{(13,34)}$=2.63; p=0.012; Nutritional state: two-way ANOVA $F_{(1,4)}$=8.69; p=0.042. (E) Representative micrograph of *Vgat^{tdTom}* cells (red) expressing c-Fos (green) in mice fasted 16h (top) and re-fed for 2h (bottom). (F) Schematic of AAV-DIO-hM3Dq-mCherry infused into NTS of *Vgat^{Cre}* mice. (G) CNO (1 mg/kg, i.p) increased NTS c-Fos (green) expression in hM3Dq-mCherry (red) of *Vgat^{Cre}* mice and (H) reduced 12h cumulative (n=6, RM two-way ANOVA ($F_{(1,10)}$=5.74; p=0.0376) and (I) 6h food intake (n=6, Unpaired t test $t_{(11)}$=2.663, p=0.0238) compared to saline treatment in GABA^{NTS}:hM3Dq mice. (J) CNO (1 mg/kg, i.p.) reduced refeeding following an overnight fast compared to saline in GABA^{NTS}:hM3Dq mice (n=6, RM two-way ANOVA $F_{(1,11)}$=10.97; P=0.0069); (K) 2h (n=6/7, Unpaired t test, $t_{(11)}$=3.392 p=0.006). (L) 10-day treatment protocol schematic. Daily CNO treatment significantly reduced (M) food intake (RM two-way ANOVA $F_{(1,11)}$=20.57; P=0.0008), (N) body weight (n=6/7, RM two-way ANOVA ($F_{(1,11)}$=21.96; p=0.0007) and (O) body weight change GABA$^{NTS:hM3Dq}$ mice compared to control GABA^{NTS}:mCherry mice (n=6/7, Unpaired t test $t_{(11)}$=5.252, p=0.0003). C-D n=4/group, H-K n=6; M-O n=6 mCherry and n=7 hM3Dq. Data represented as mean±S.E.M. *: p<0.05; **: p<0.01; ***: p<0.001. AP: Area Postrema; CC: Centre canal; DMV: Doral motor nucleus of the vagus nerve; NTS: Nucleus of the solitary tract.

Figure 2. GABA^{NTS} projections to the ARC release GABA into AgRP/NPY neurons. (A) Illustration depicting details for NTS injection of AAV-DIO-ChR2-mCherry (top) and representative photomicrograph (scale 1mm) of injection (bottom) in *Vgat^{Cre}* mice and (B) ChR2-mcherry containing fibers in the ARC (scale 200um). (B) Representative photomicrographs (scale 100um) and magnification (scale 50 and 10um) ChR2-mCherry fibers in the ARC close to NPY^{hrGFP}-expressing cells and (D) POMC-expressing cells and in *Vgat^{Cre}* mice bilaterally injected AAV-DIO-ChR2-mCherry. (E-G) *Vgat^{Cre}*:*Npy^{hrGFP}* mice CRACM study. (E) Representative membrane current in Npy^{hrGFP} cell recorded during a voltage-clamp experiment from -100mV to -10mV in 10-mV steps. (Vertical line: light pulse; green cross: base line; red cross: peak value). (F) Representative light-induced post-synaptic current during voltage clamp experiment showing peak conductance, G_s, and reversal potential, E_{rev}. (G) Individual values and median of E_{rev}, G_s and latency of all responsive cells. (H) Diagram of outside-out patch technique in *Vgat^{Cre}*:*Npy^{hrGFP}* mice bilaterally injected AAV-DIO-ChR2-mCherry. (I) Representative channel opening recordings of control (top) gabazine (middle) and washout (bottom) recordings. (J) Quantification of receptor opening time (n=4, RM two-way ANOVA $F_{(2,6)}$=16.14; p=0.0039, Bonferroni adjusted p=0.0051 Control vs Gabazine and p=0.0156 Gabazine vs Washout). (K) Diagram of outside-out patch technique coupled to a postsynaptic electrical stimulator. (L, top) Representative response of Npy^{hrGFP} cell subjected to series of five electrical stimuli, each evoking excitatory post-synaptic potential (EPSP) of sub-threshold amplitude and (L, bottom) same cell with electrical stimuli coupled with 470nm light burst. (M) Quantification of receptor opening time (n=5, two-way RM ANOVA $F_{(2,8)}$=11.28; p=0.0047, Bonferroni adjusted p=0.0072 NS vs SL and p=0.0157 S vs SL). Data in J and M are expressed as mean±S.E.M. E-G: 4/27 cells; I-J: n=4-5 patches, L-M n=4-5 cells. *: p<0.05; **: p<0.01. NS: No stimulation; S: Stimulation; SL: Stimulation+Light.

Figure 3. Activation of GABA^{NTS}→ARC projections reduces food intake without inducing aversion. (A) Schematic of viral infection and optic fiber placement for in vivo stimulation of GABA^{NTS}→ARC. (B) Protocol of stimulation. (C) Representative 1min resolution time plot of 3h food intake measurement. GABA^{NTS}→ARC stimulation significantly reduces (D) cumulative 3h food intake and (E) 60min intake (n=7, day 1 (OFF) vs day 2 (ON) paired Student t-test $t_{(6)}$=3.035, p=0.0229; day 2 (ON) vs day 3 (OFF) paired Student t-test $t_{(6)}$=3.283, p=0.0168). (F) Diagram illustrating RTPP task. GABA^{NTS}→ARC does not alter (G) time spent (representative heat map of time) or (H) distance travelled in stimulated and non-stimulated zones. (I) Diagram illustrating an object interaction task. (J) Interactions with novel, known nutritional or novel palatable objects and a representative path track around each object (red circle). GABA^{NTS}→ARC stimulation reduced interaction with known nutritional item (n=6, Student's t test $t_{(5)}$=3.043, p=0.0287). Data are expressed as individual values and as mean±S.E.M, n=6 mice. *: p<0.05; RTPP: real-time place preference.

Figure 4. Chemogenetic activation of GABA^{NTS}→ARC neurons induces satiety. (A) Diagram illustrating the two-virus intersectional strategy to express hM3Dq only in GABA^{NTS} neurons projecting to the ARC. Mice were treated with saline or CNO (1 mg/kg, i.p.). (B) CNO significantly reduced cumulative food intake over 6h (0-6h $F_{(1,15)}$=7.418, p=0.0157), (C) 1h (Unpaired t-test $t_{(15)}$=2.648, p=0.0183) and 3h (Unpaired t-test, $t_{(15)}$=2.568 P=0.0214) food intake compared to saline. (D) CNO did not alter 12h or (E) 1, 3, 6 or 12h quantification of ambulation; (F) 12h RER or (G) AUC quantification; (H) 12h or (I) 1, 3, 6 and 12h heat production per mouse compared to saline. (J-K) CNO significantly reduced 3h food intake following overnight fasting (J, 2-way ANOVA $F_{(1.13)}$=6.139, p=0.0277 and K, unpaired t-test $t_{(13)}$=2.320, p=0.0372). (L-M) CNO attenuated ghrelin hyperphagia over 2h (RM ANOVA $F_{(3,16)}$=11.12; p=0.0003, Bonferroni adjusted p=0.0042 control vs ghrelin, p=0.0003 CNO vs ghrelin and p=0.002 Ghrelin vs Ghrelin+CNO). (N) CNO reduced meal size (Unpaired t-test, $t_{(14)}$=2.256, p=0.0406) and (O-P) decreased meal number (Unpaired t-test, t(14)=2.824, p=0.0135) compared to control. Data are expressed as individual values and as mean±SEM. *: p<0.05; **: p<0.01. ***: p<0.001.

Figure S1. GABA^{NTS} projection pattern and CRACM additional analysis. (A) Representative photomicrographs (scale 100µm) of ChR2-mCherry fibers in a serial rostro-caudal distribution of a *Vgat^{Cre}* mouse brain injected with AAV-DIO-ChR2-mCherry into the NTS. (B) Representative response of a single Npy^{hrGFP} cell subjected to 10 series of five electrical stimuli, each evoking excitatory post-synaptic potential (EPSP) of sub-threshold amplitude coupled with 470nm light burst in *Vgat^{Cre}:NPY^{hrGFP}* mouse injected with AAV-DIO-ChR2-mCherry into the NTS. (C-F) A simulated voltage-clamp experiment in an anatomically realistic model of a medium spiny neuron, using the same voltage steps as those described for electrophysiology experiments (Figure 2E-G). The effect of optogenetic stimulation was modelled as a single GABAergic event taking place at each step. (D) Current amplitude was plotted against voltage (as in Figure 2E-G), and a linear fit was used to estimate peak conductance G_s and reversal potential E_{rev}. (E-F) Simulated optogenetic activation of GABA inputs making synaptic contact only on dendrites close to the soma ("prox.", proximal dendrites) was compared to the same type of activation of GABA synapses connected only to dendrites far from the soma ("distal" dendrites) in six different medium spiny neuron models. The reversal potential for GABA in the model was set to -60 mV, and this is close to what was measured at the soma when GABA synaptic inputs were located on dendrites close to the soma. However, when GABA synapses were activated only on dendrites distant from the soma E_{rev}, was more positive than expected and conductance G_s was attenuated.

Figure S2. Optogenetic activation of GABA^{NTS}→ARC in *Vgat^{Cre}* mice does not induce anxiety-like behavior. (A) Diagram illustrating open field arena (OFA) task. GABA^{NTS}→ARC does not alter (B) time spent in the center or (C) distance travelled (representative trace of the movement) during the test. (D) Diagram illustrating elevated zero maze (EZM) task. GABA^{NTS}→ARC does not alter (E) time spent in the exposed area or (F) distance travelled in each zone (representative trace of the movement) during the test. (G-H) Quantification of number of interactions with a novel object, a known nutritional food item or a novel palatable food item in mice (G) non-stimulated (RM ANOVA ($F_{(2,10)}$=4.993; p=0.0314, Bonferroni adjusted p=0.0306 NO vs NP) and (H) stimulated (RM ANOVA $F_{(2,10)}$=10.71; p=0.0033, Bonferroni adjusted p=0.0051 NO vs NP; p=0.0121 KN vs NP). Data are expressed as individual values and as mean±S.E.M, n=6 mice. *:p<0.05; **:p<0.01. NO: novel object; NP: novel palatable; KN: known nutritional.

REFERENCES

1. Campos, A., Port, J. D. & Acosta, A. Integrative Hedonic and Homeostatic Food Intake Regulation by the Central Nervous System: Insights from Neuroimaging. *Brain Sci* **12**, (2022).

2. Andermann, M. L. & Lowell, B. B. Toward a Wiring Diagram Understanding of Appetite Control. *Neuron* **95**, 757–778 (2017).

3. Hyun, U. & Sohn, J. W. Autonomic control of energy balance and glucose homeostasis. *Experimental & Molecular Medicine 2022 54:4* **54**, 370–376 (2022).

4. Ludwig, M. Q. *et al.* A genetic map of the mouse dorsal vagal complex and its role in obesity. *Nat Metab* **3**, 530–545 (2021).

5. Dowsett, G. K. C. *et al.* A survey of the mouse hindbrain in the fed and fasted states using single-nucleus RNA sequencing. *Mol Metab* **53**, 101240 (2021).

6. Grill, H. J. & Hayes, M. R. Hindbrain Neurons as an Essential Hub in the Neuroanatomically Distributed Control of Energy Balance. *Cell Metab* **16**, 296–309 (2012).

7. Cheng, W. *et al.* Leptin receptor-expressing nucleus tractus solitarius neurons suppress food intake independently of GLP1 in mice. *JCI Insight* **5**, (2020).

8. Cheng, W. *et al.* Calcitonin Receptor Neurons in the Mouse Nucleus Tractus Solitarius Control Energy Balance via the Non-aversive Suppression of Feeding. *Cell Metab* **31**, 301-312.e5 (2020).

9. Alhadeff, A. L. *et al.* Endogenous Glucagon-like Peptide-1 Receptor Signaling in the Nucleus Tractus Solitarius is Required for Food Intake Control. *Neuropsychopharmacology* **42**, 1471–1479 (2017).

10. Fortin, S. M. *et al.* GABA neurons in the nucleus tractus solitarius express GLP-1 receptors and mediate anorectic effects of liraglutide in rats HHS Public Access. *Sci Transl Med* **12**, 109–114 (2020).

11. Holt, M. K. *et al.* Preproglucagon neurons in the nucleus of the solitary tract are the main source of brain GLP-1, mediate stress-induced hypophagia, and limit unusually large intakes of food. *Diabetes* **68**, 21–33 (2019).

12. Aklan, I. *et al.* NTS Catecholamine Neurons Mediate Hypoglycemic Hunger via Medial Hypothalamic Feeding Pathways. *Cell Metab* **31**, 313-326.e5 (2020).

13. Chen, J. *et al.* A Vagal-NTS Neural Pathway that Stimulates Feeding. *Current Biology* **30**, 3986-3998.e5 (2020).

14. D'Agostino, G. *et al.* Appetite controlled by a cholecystokinin nucleus of the solitary tract to hypothalamus neurocircuit. *Elife* **5**, (2016).

15. Zhan, C. *et al.* Acute and long-term suppression of feeding behavior by POMC neurons in the brainstem and hypothalamus, respectively. *J Neurosci* **33**, 3624–3632 (2013).

16. Georgescu, T. *et al.* Neurochemical Characterization of Brainstem Pro-Opiomelanocortin Cells. *Endocrinology* **161**, (2020).

17. Shi, M. Y. *et al.* Long-range GABAergic projections from the nucleus of the solitary tract. *Mol Brain* **14**, 1–5 (2021).

18. Blevins, J. E., Schwartz, M. W. & Baskin, D. G. Evidence that paraventricular nucleus oxytocin neurons link hypothalamic leptin action to caudal brain stem nuclei controlling meal size. *Am J Physiol Regul Integr Comp Physiol* **287**, 87–96 (2004).

19. Liu, J. *et al.* Enhanced AMPA receptor trafficking mediates the anorexigenic effect of endogenous glucagon like peptide-1 in the paraventricular hypothalamus. *Neuron* **96**, 897 (2017).

20. Tsang, A. H., Nuzzaci, D., Darwish, T., Samudrala, H. & Blouet, C. Nutrient sensing in the nucleus of the solitary tract mediates non-aversive suppression of feeding via inhibition of AgRP neurons. *Mol Metab* **42**, 101070 (2020).

21. Betley, J. N., Cao, Z. F. H., Ritola, K. D. & Sternson, S. M. Parallel, Redundant Circuit Organization for Homeostatic Control of Feeding Behavior. *Cell* **155**, 1337–1350 (2013).

22. Heisler, L. K. & Lam, D. D. An appetite for life: brain regulation of hunger and satiety. *Curr Opin Pharmacol* **37**, 100–106 (2017).

23. Heisler, L. K. *et al.* Serotonin Reciprocally Regulates Melanocortin Neurons to Modulate Food Intake. *Neuron* **51**, 239–249 (2006).

24. Hahn, T. M., Breininger, J. F., Baskin, D. G. & Schwartz, M. W. Coexpression of Agrp and NPY in fasting-activated hypothalamic neurons. *Nature Neuroscience 1998 1:4* **1**, 271–272 (1998).

25. Olson, B. R. *et al.* C-Fos expression in rat brain and brainstem nuclei in response to treatments that alter food intake and gastric motility. *Mol Cell Neurosci* **4**, 93–106 (1993).

26. Alexander, G. M. *et al.* Remote control of neuronal activity in transgenic mice expressing evolved G protein-coupled receptors. *Neuron* **63**, 27–39 (2009).

27. Petreanu, L., Huber, D., Sobczyk, A. & Svoboda, K. Channelrhodopsin-2-assisted circuit mapping of long-range callosal projections. (2007) doi:10.1038/nn1891.

28. González, J. A., Iordanidou, P., Strom, M., Adamantidis, A. & Burdakov, D. Awake dynamics and brain-wide direct inputs of hypothalamic MCH and orexin networks. *Nat Commun* **7**, (2016).

29. Aponte, Y., Atasoy, D. & Sternson, S. M. AGRP neurons are sufficient to orchestrate feeding behavior rapidly and without training. *Nature Neuroscience 2011 14:3* **14**, 351–355 (2011).

30. Krashes, M. J. *et al.* Rapid, reversible activation of AgRP neurons drives feeding behavior in mice. *Journal of Clinical Investigation* **121**, 1424–1428 (2011).

31. Krnjević, K. & Schwartz, S. The action of γ-Aminobutyric acid on cortical neurones. *Exp Brain Res* **3**, 320–336 (1967).

32. Williams, D. L. & Schwartz, M. W. The melanocortin system as a central integrator of direct and indirect controls of food intake. *Am J Physiol Regul Integr Comp Physiol* **289**, (2005).

33. Spruston, N., Jaffe, D. B., Williams, S. H. & Johnston, D. Voltage- and space-clamp errors associated with the measurement of electrotonically remote synaptic events. *J Neurophysiol* **70**, 781–802 (1993).

34. Lindroos, R. & Hellgren Kotaleski, J. Predicting complex spikes in striatal projection neurons of the direct pathway following neuromodulation by acetylcholine and dopamine. *Eur J Neurosci* **53**, 2117–2134 (2021).

35. Sylantyev, S., Savtchenko, L. P., O'Neill, N. & Rusakov, D. A. Extracellular GABA waves regulate coincidence detection in excitatory circuits. *J Physiol* **598**, 4047 (2020).

36. D'Agostino, G. & Luckman, S. M. Brainstem peptides and peptidergic neurons in the regulation of appetite. *Curr Opin Endocr Metab Res* **24**, 100339 (2022).

37. Betley, J. N. *et al.* Neurons for hunger and thirst transmit a negative-valence teaching signal. *Nature* **521**, 180 (2015).

38. Berridge, K. C. Motivation concepts in behavioral neuroscience. *Physiol Behav* **81**, 179–209 (2004).

39. Stamatakis, A. M. & Stuber, G. D. Activation of lateral habenula inputs to the ventral midbrain promotes behavioral avoidance. *Nature Neuroscience 2012 15:8* **15**, 1105–1107 (2012).

40. Kim, S. Y. *et al.* Diverging neural pathways assemble a behavioural state from separable features in anxiety. *Nature 2013 496:7444* **496**, 219–223 (2013).

41. Li, C. *et al.* AGRP neurons modulate fasting-induced anxiolytic effects. *Translational Psychiatry 2019 9:1* **9**, 1–10 (2019).

42. Dietrich, M. O., Zimmer, M. R., Bober, J. & Horvath, T. L. Hypothalamic Agrp Neurons Drive Stereotypic Behaviors beyond Feeding. *Cell* **160**, 1222–1232 (2015).

43. Heinz, D. E. *et al.* Exploratory drive, fear, and anxiety are dissociable and independent components in foraging mice. *Translational Psychiatry 2021 11:1* **11**, 1–12 (2021).

44. Fenno, L. E., Mattis, J., Ramakrishnan, C. & Deisseroth, K. A Guide to Creating and Testing New INTRSECT Constructs. *Curr Protoc Neurosci* **80**, 4.39.1-4.39.24 (2017).

45. Fenno, L. E. *et al.* Targeting cells with single vectors using multiple-feature Boolean logic. *Nat Methods* **11**, 763–772 (2014).

46. Cummings, D. E. *et al.* A Preprandial Rise in Plasma Ghrelin Levels Suggests a Role in Meal Initiation in Humans. *Diabetes* **50**, 1714–1719 (2001).

47. Chen, H. Y. *et al.* Orexigenic Action of Peripheral Ghrelin Is Mediated by Neuropeptide Y and Agouti-Related Protein. *Endocrinology* **145**, 2607–2612 (2004).

48. Luquet, S., Phillips, C. T. & Palmiter, R. D. NPY/AgRP neurons are not essential for feeding responses to glucoprivation. *Peptides (N.Y.)* **28**, 214–225 (2007).

49. Clifton, P. G. Meal patterning in rodents: psychopharmacological and neuroanatomical studies. *Neurosci Biobehav Rev* **24**, 213–222 (2000).

50. Richard, C. D., Tolle, V. & Low, M. J. Meal pattern analysis in neural-specific proopiomelanocortin-deficient mice. *Eur J Pharmacol* **660**, 131–138 (2011).

51. Zorrilla, E. P. *et al.* Measuring meals: Structure of prandial food and water intake of rats. *Am J Physiol Regul Integr Comp Physiol* **288**, 1450–1467 (2005).

52. Cheng, W. *et al.* Hindbrain circuits in the control of eating behaviour and energy balance. *Nat Metab* **4**, 826–835 (2022).

53. Wu, Q. *et al.* The Temporal Pattern of cfos Activation in Hypothalamic, Cortical, and Brainstem Nuclei in Response to Fasting and Refeeding in Male Mice. *Endocrinology* **155**, 840–853 (2014).

54. D'Agostino, G. *et al.* Nucleus of the Solitary Tract Serotonin 5-HT2C Receptors Modulate Food Intake. *Cell Metab* **28**, 619-630.e5 (2018).

55. Aponte, Y., Atasoy, D. & Sternson, S. M. AGRP neurons are sufficient to orchestrate feeding behavior rapidly and without training. *Nat Neurosci* **14**, 351–355 (2011).

56. Luquet, S., Perez, F. A., Hnasko, T. S. & Palmiter, R. D. NPY/AgRP neurons are essentials for feeding in adult mice but can be ablated in neonates. *Science (1979)* **310**, 683–685 (2005).

57. Berrios, J. *et al.* Food cue regulation of AGRP hunger neurons guides learning. *Nature* **595**, 695 (2021).

58. Deem, J. D., Faber, C. L. & Morton, G. J. AgRP neurons: Regulators of feeding, energy expenditure, and behavior. *FEBS Journal* **289**, 2362–2381 (2022).

59. Dietrich, M. O. *et al.* AgRP neurons regulate development of dopamine neuronal plasticity and nonfood-associated behaviors. *Nat Neurosci* (2012) doi:10.1038/nn.3147.

60. Garau, C., Blomeley, C., Burdakov, D. & Burdakov, D. Orexin neurons and inhibitory Agrp→orexin circuits guide spatial exploration in mice. *J Physiol* **598**, 4371–4383 (2020).

61. Han, Y. *et al.* Deciphering an AgRP-serotoninergic neural circuit in distinct control of energy metabolism from feeding. *Nature Communications 2021 12:1* **12**, 1–16 (2021).

62. Jikomes, N., Ramesh, R. N., Mandelblat-Cerf, Y. & Andermann, M. L. Preemptive Stimulation of AgRP Neurons in Fed Mice Enables Conditioned Food Seeking under Threat. *Current Biology* **26**, 2500–2507 (2016).

63. Krashes, M. J. *et al.* An excitatory paraventricular nucleus to AgRP neuron circuit that drives hunger. *Nature 2014 507:7491* **507**, 238–242 (2014).

64. Wang, C. *et al.* AgRP neurons trigger long-term potentiation and facilitate food seeking. *Transl Psychiatry* **11**, 11 (2021).

65. Vong, L. *et al.* Leptin action on GABAergic neurons prevents obesity and reduces inhibitory tone to POMC neurons. *Neuron* **71**, 142–154 (2011).

66. van den Pol, A. N. *et al.* Neuromedin B and gastrin-releasing peptide excite arcuate nucleus neuropeptide Y neurons in a novel transgenic mouse expressing strong Renilla green fluorescent protein in NPY neurons. *J Neurosci* **29**, 4622–4639 (2009).

67. Madisen, L. *et al.* A robust and high-throughput Cre reporting and characterization system for the whole mouse brain. *Nature Neuroscience 2009 13:1* **13**, 133–140 (2009).

68. Zingg, B. *et al.* AAV-Mediated Anterograde Transsynaptic Tagging: Mapping Corticocollicular Input-Defined Neural Pathways for Defense Behaviors. *Neuron* **93**, 33–47 (2017).

69. Wagner, S. *et al.* Obesity medication lorcaserin activates brainstem GLP-1 neurons to reduce food intake and augments GLP-1 receptor agonist induced appetite suppression. *Mol Metab* **68**, (2022).

70. Lin, J. Y., Lin, M. Z., Steinbach, P. & Tsien, R. Y. Characterization of Engineered Channelrhodopsin Variants with Improved Properties and Kinetics. *Biophys J* **96**, 1803–1814 (2009).

71. Yavari, A. *et al.* Chronic Activation of gamma2 AMPK Induces Obesity and Reduces beta Cell Function. *Cell Metab* **23**, 821–836 (2016).